




Cite this: *Biomater. Sci.*, 2019, 7, 5283

Combretastatin A4 nanodrug combined plerixafor for inhibiting tumor growth and metastasis simultaneously

Jian Jiang, ^{a,b,c} Na Shen,^{a,c} Wantong Song,^{a,c} Haiyang Yu,^{a,c} Kazuo Sakurai, ^d Zhaohui Tang ^{*a,c} and Gao Li^{a,c}

Inhibition of tumor growth and metastasis simultaneously is an important issue for tumor therapy. The CXCR4/CXCL12 axis plays a crucial role in cancer metastasis, and the blocking of the CXCR4/CXCL12 axis is an effective way of inhibiting cancer metastasis. Combretastatin A4 nanodrug (CA4-NPs), a neogenesis blood vascular disrupting agent, can accumulate around blood vessels and disrupt tumor neogenesis of blood vessels more efficaciously than typical small molecular drug combretastatin A4 phosphate (CA4P). However, in this work, we find that the CXCR4 expression is significantly enhanced in CA4-NPs-treated tumor tissues in a metastatic orthotopic 4T1 mammary adenocarcinoma mouse model. Considering that the overexpression of CXCR4 can promote tumor cell metastasis, a novel cooperative strategy that utilizes plerixafor (PLF, CXCR4 antagonist) with CA4-NPs for inhibiting tumor growth and metastasis simultaneously is developed. The combination of CA4-NPs (60 mg kg⁻¹ on CA4 basis) + PLF shows remarkably enhanced antitumor efficacy. The tumor growth inhibition rate of the combination group reaches 91.3%, significantly higher than those of non-cooperative groups. In addition, the number of lung metastasis foci of the combination group is least among all groups. This cooperative strategy provides a useful method for inhibiting tumor growth and metastasis simultaneously, and gives the evidence to support the clinical use of the combination of vascular disruption agents and CXCR4 antagonists.

Received 4th September 2019,
Accepted 25th September 2019

DOI: 10.1039/c9bm01418g

rsc.li/biomaterials-science

1. Introduction

Metastasis is responsible for as much as 90% of cancer-associated mortality.^{1,2} Inhibition of tumor growth and metastasis simultaneously is an important issue for tumor therapy and has received increasing attention.^{3–5} The CXCR4/CXCL12 axis plays an important role in cancer metastasis as previously reported.^{6–9} Under normal conditions, the autologous stem-cell transplantation is dependent on the CXCR4/CXCL12 axis. The stem cells express chemokine receptor CXCR4 which has the ability to induce directional migration toward a gradient of CXCR4-specific ligand stromal cell-derived factor-1 α (CXCL12).^{10,11} Malignant breast cancer cells are reported to be able to express the chemokine receptor CXCR4 and commonly metastasize to organs that are an abundant source of CXCL12.^{12,13} Therefore,

the blocking of the CXCR4/CXCL12 axis is an effective way of inhibiting cancer metastasis in tumor therapy.

Vascular disrupting agents (VDAs) can modulate the tumor microenvironment selectively through eliminating the immature blood vessels in tumors preferentially.^{14–16} Combretastatin A4 phosphate (CA4P), as a representative small-molecular-weight VDA, could elicit extensive tumor necrosis, leaving normal tissues relatively impregnable.^{17–19} Recently, a combretastatin A4 nanodrug (CA4-NPs) was developed which exhibited higher selectivity to blood vessels in tumors compared to CA4P for strong tumor growth inhibition.^{20–23} However, in this study, we found that the treatment with CA4-NPs could induce the overexpression of CXCR4 in tumor tissues in the orthotopic 4T1 mammary adenocarcinoma mouse model. This phenomenon reveals that the blocking of the CXCR4/CXCL12 axis is necessary during CA4-NPs tumor therapy for inhibiting tumor growth and metastasis simultaneously.

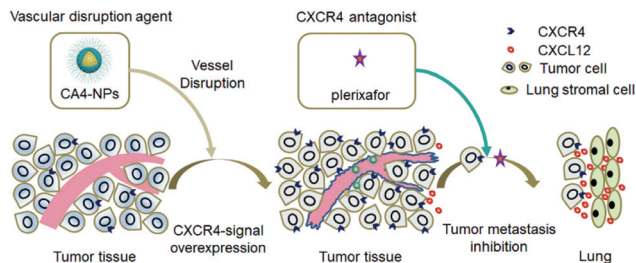
Therefore, a cooperative strategy utilizing plerixafor (PLF) with CA4-NPs is developed. Plerixafor (also termed AMD3100), a CXCR4 antagonist, was approved by the FDA for Multiple Myeloma and Non-Hodgkin's Lymphoma in mobilizing hematopoietic stem cells for autologous stem-cell transplantation through subcutaneous injection.^{24,25} Herein, CA4-NPs are used

^aKey Laboratory of Polymer Ecomaterials, Changchun Institute of Applied Chemistry, Chinese Academy of Sciences, Changchun 130022, P. R. China.
E-mail: ztang@ciac.ac.cn

^bSchool of Applied Chemistry and Engineering, University of Sciences and Technology of China, Hefei 230026, P. R. China

^cJilin Biomedical Polymers Engineering Laboratory, Changchun, 130022, P. R. China

^dThe University of Kitakyushu, Department of Chemistry and Biochemistry, 1-1, Hibikino, Wakamatsu-ku, Kitakyushu, Fukuoka, 808-0135, Japan



Scheme 1 Illustration of cooperative cancer treatment by combining combretastatin A4 nanodrug with plerixafor. CA4-NPs disrupt tumor vasculature and induce the overexpression of CXCR4 in the treated tumors. Blocking of the CXCR4/CXCL12 axis with plerixafor (CXCR4 antagonist) could inhibit tumor cell metastasis to distant organs (such as lung, etc.) which express a high level of CXCL12.

to disrupt tumor vasculature for strong tumor growth inhibition. However, the overexpression of CXCR4 in CA4-NPs-treated tumors could promote tumor cell metastasis to distant organs that express a high level of CXCL12. So, plerixafor is combined with CA4-NPs in the treatment for blocking the CXCR4/CXCL12 axis to inhibit tumor cell metastasis (Scheme 1). *In vivo* results reveal that this cooperative strategy can inhibit tumor growth and metastasis simultaneously. This work provides a useful strategy for inhibiting tumor growth and metastasis simultaneously and gives the evidence to support the clinical combination use of vascular disruption agents and CXCR4 antagonists.

2. Experimental

2.1 Materials

Poly(L-glutamic acid)-*g*-methoxy poly(ethylene glycol), PLG₁₆₀-*g*-mPEG_{5k}, also termed PLG-*g*-mPEG, was prepared as described previously.²⁶ The average number of L-glutamic acid repeating units and mPEG_{5k} chains in PLG₁₆₀-*g*-mPEG_{5k} equaled 160 and 8.3, respectively. Plerixafor (PLF, Shanghai Send Pharmaceutical Technology Co., Ltd, China), combretastatin A4 (CA4, Hangzhou Great Forest Biomedical Ltd, China), 4',6-diamidino-2-phenylindole dihydrochloride (DAPI, Sigma-Aldrich, USA) were used as received. *N,N*-Dimethylformamide (DMF) was purified by vacuum distillation over calcium hydride (CaH₂). FITC-labeled anti-CXCR4 primary antibody (551967) was purchased from BD Pharmingen™ (USA). Anti-CXCR4 primary antibody (14-9991-82) was purchased from eBioscience (USA) and FITC-labeled anti-rat secondary antibody (a0192) was purchased from Beyotime Biotechnology (China). APC-labeled anti-CD31 primary antibody (17-0311-80) was purchased from eBioscience (USA). Anti-HIF-1α primary antibody (NB100-105) was purchased from Novus Biologicals, Inc. (USA). FITC-labeled anti-mouse secondary antibody (a0568) was purchased from Beyotime Biotechnology (China). Anti-mouse β-actin primary antibody (HC201-01) was purchased from TransGen Biotech (Beijing, China). Deionized water was prepared using a Milli-Q plus system (Millipore Co.,

Billerica, MA, USA). 1× cell lysis buffer (C500035-0010) was purchased from Sangon Biotech (Shanghai, China). All the other reagents and solvents were purchased from Sinopharm Chemical Reagent Co. Ltd (China) and used as received.

2.2 Characterization

¹H NMR spectrum was recorded using an AV-300 NMR spectrometer (Bruker, Karlsruhe, Germany) in deuterated water (D₂O) with a little NaOD. The diameter of the nanoparticles was measured by dynamic light scattering (DLS) using a Zetasizer pro system (Malvern Panalytical Ltd, UK). Gel permeation chromatography (GPC) was conducted using a Waters GPC system, containing a Waters Ultrahydrogel Linear column, a 1515 HPLC pump and a 2414 Refractive Index detector. The mobile phase consisted of phosphate buffer (0.2 M, pH 7.4) pumped at a flow rate of 1.0 mL min⁻¹ and polyethylene glycol was used as standards. The ultraviolet-visible (UV-vis) absorption spectrum was recorded using a UV-2401PC spectrophotometer (Shimadzu, Japan). A high-performance liquid chromatography (HPLC) system comprised a reverse-phase C18 column (symmetry, 5 μm, 4.6 mm × 250 mm), a Waters 1525 Binary HPLC pump and a UV-Vis detector to quantify the CA4 content loaded within the nanoparticles. The mobile phase consisted of acetonitrile and water (at a ratio of 4/1, v/v) pumped at a flow rate of 1.0 mL min⁻¹. The absorption wavelength of the sample of CA4-NPs was set at 305 nm. A confocal laser scanning microscope (Zeiss LSM 780, Germany) was used to detect the expression of CXCR4, CD31 and HIF-1α in tumor tissues or tumor cells.

2.3 Preparation of CA4-NPs

For the preparation of poly(L-glutamic acid)-*graft*-methoxy poly(ethylene glycol)/combretastatin A4 (abbreviated as PLG-*g*-mPEG/CA4), CA4 was grafted onto PLG-*g*-mPEG through the Yamaguchi reaction, as previously reported.²⁰ In brief, PLG-*g*-mPEG (2.2 g) was dissolved in 25.0 mL anhydrous DMF. CA4 (0.6 g, 0.5 mmol), 2,4,6-trichlorobenzoyl chloride (0.9 g, 1.0 mmol), DMAP (0.25 g, 0.6 mmol) and triethylamine (0.37 mg, 1.0 mmol) were dissolved in 10.0 mL anhydrous DMF and then this DMF solution was added into the above PLG-*g*-mPEG solution. The reaction mixture was precipitated into excess diethyl ether after processing at 60 °C for 5 h. The white precipitate was dried under vacuum and redissolved in DMF. After dialyzing against distilled water (MWCO 3500 Da), the final product (PLG-*g*-mPEG/CA4) was obtained after lyophilization. The PLG-*g*-mPEG/CA4 could self-assemble to form CA4-loaded nanoparticles (CA4-NPs). PLG-*g*-mPEG/CA4 and free CA4 contents were measured using HPLC with a UV-Vis detector. Drug loading content (DLC%) and drug loading efficiency (DLE%) were calculated based on the following equations:

$$\text{DLC}\% = \frac{\text{CA4 weight}}{\text{Total CA4-NPs weight}} \times 100\%$$

$$\text{DLE}\% = \frac{\text{CA4 weight}}{\text{Theoretical CA4 weight}} \times 100\%$$

2.4 *In vitro* drug release

In vitro drug release was investigated in 0.07 M PBS containing 0.2% (w/v) Tween 80. 3.0 mg CA4-NPs were dissolved in 3.0 mL release medium and placed into a dialysis bag (MWCO 3500 Da). The dialysis bag was then transferred into 27.0 mL of release medium and placed into a thermostatic tank which was gently shaken at 100 rpm at 37 °C. At specified time intervals, 3.0 mL of release solution was collected and replaced with an equal volume of fresh release medium.

2.5 Cell culture

Mouse triple negative breast carcinoma 4T1 cells were cultured in Dulbecco's modified Eagle's medium (DMEM), which contained 10% fetal bovine serum (FBS), 50.0 U mL⁻¹ penicillin and 50.0 U mL⁻¹ streptomycin. The 4T1 cells were incubated at 37 °C in an atmosphere containing 5% CO₂.

2.6 RNA extraction and real time polymerase chain reaction (PCR)

Relative CXCR4 and HIF-1 α mRNA expression were quantified by real time PCR. The total RNA extraction kit (Tiangen) was used for extracting total RNA from cells. cDNA was synthesized using a reverse transcription kit (Tiangen). The gene expression was quantified using a SYBR green real time PCR kit (Tiangen). GAPDH was used as an internal reference. The primers used were listed below:

Mouse CXCR4 (Forward: 5'-TCAGTGGCTGACCTCCTCTT-3', Reverse: 5'-CTTGGCCTTTGACTGTTGGT-3');

Mouse HIF-1 α (Forward: 5'-CCTGCACTGAATCAAGAG-GTTGC-3', Reverse: 5'-CCATCAGAAGGACTTGCTGGCT-3');

Mouse GAPDH (Forward: 5'-AGTGGCAAAGTGGAGATT-3', Reverse: 5'-GTGGAGTCATACTGGAACA-3').

2.7 Animals

Female BALB/c mice (6–8 weeks old) were purchased from Beijing Vital River Laboratory Animal Technology Co., Ltd. All animal procedures were performed in accordance with the Guidelines for Care and Use of the Laboratory Animals of Jilin University and experiments were approved by the Animal Ethics Committee of Jilin University.

2.8 *In vivo* antitumor efficacy

4T1 cells (2.0×10^6 in 0.1 mL PBS) were injected in the right mammary fat pad of each mouse for establishing the orthotopic triple negative breast cancer tumor model. When the tumor volume reached approximately 150 mm³, mice were randomly divided into 6 groups ($n = 6$): PBS; PLF (2.5 mg kg⁻¹ on PLF basis), termed PLF; CA4-NPs (30 mg kg⁻¹ on CA4 basis), termed CA4-NPs (30); CA4-NPs (30 mg kg⁻¹ on CA4 basis) + PLF (2.5 mg kg⁻¹ on PLF basis), termed CA4-NPs (30) + PLF; CA4-NPs (60 mg kg⁻¹ on CA4 basis), termed CA4-NPs (60); CA4-NPs (60 mg kg⁻¹ on CA4 basis) + PLF (2.5 mg kg⁻¹ on PLF basis), termed CA4-NPs (60) + PLF. The start of treatment was recorded as day 1. CA4-NPs were injected intravenously *via* the tail vein on day 1 and/or 7. PLF was injected everyday intraperi-

toneally into mice. Tumor volume and body weight were monitored to evaluate the tumor therapy efficacy and systematic toxicity. The tumor volume (mm³) was calculated based on the following equation:

$$V = \frac{ab^2}{2}$$

where a and b represent the longest and shortest diameter of the tumor, respectively. At the end point of the treatment, the mice were sacrificed. The tumors and major organs, including heart, liver, spleen, lung and kidney were excised for histopathological analysis.

Tumor inhibition rate was calculated at the end of the treatment using the following equation:

$$\begin{aligned} \text{Tumor inhibition rate (\%)} \\ = 100 - (\text{experimental tumor volume} / \text{control tumor volume}) \\ \times 100 \end{aligned}$$

The Q value method²⁷ was used to evaluate the synergistic interaction of the combination group with CA4-NPs and PLF for tumor therapy. The Q value was calculated using the following equation:

$$Q = \frac{E_{(A+B)}}{E_{(A)} + E_{(B)} - E_{(A)} \times E_{(B)}}$$

where $E_{(A+B)}$, $E_{(A)}$ and $E_{(B)}$ represent the tumor inhibition rate of the combination group of A + B, group A and group B respectively. $Q < 0.85$ reveals the antagonism effect of the combination A + B. $0.85 \leq Q < 1.15$ reveals the additive effect of the combination A + B. $1.15 \leq Q$ reveals the synergistic effect of the combination A + B.

2.9 Immunofluorescence staining assay

The expressions of CXCR4, CD31 and HIF-1 α were analyzed by immunofluorescence staining assay. The tumor tissues were excised and fixed in 4% buffered paraformaldehyde for 24 h, then embedded in paraffin and sliced to a thickness of 5.0 μ m. The tumor tissue slides were deparaffinized by xylene, hydrated through a gradient of alcohol, boiled in 0.01 M sodium citrate buffer (pH 6.0) for antigen retrieval. After treating in blocking medium (5% BSA PBS buffer) for 20 min, the tumor tissue slices were first incubated with a monoclonal primary antibody (CXCR4, CD31 or HIF-1 α), and incubated with or without a fluorescently labelled secondary antibody, then imaged by confocal laser scanning microscopy (CLSM).

2.10 Histopathology imaging

The tumors and the major organs from mice at the end point treatment were excised, fixed in 4% buffered paraformaldehyde, embedded in paraffin, sliced to a thickness of 5.0 μ m, and stained with hematoxylin and eosin (H&E) to evaluate the histopathological changes using an inverted fluorescent microscope (Nikon TE2000U).

2.11 Western blotting

Western blot assay^{28,29} was used to analyze the relative expression of CXCR4 and HIF-1 α of cells or tumor tissues. The cells were prepared by lysing in 1 \times cell lysis buffer in the *in vitro* studies. The supernatant of cell-lysis buffer was collected after centrifugation at 13 800g for 2 min. Tumor tissues (~150 mm³) with different treatments for 48 h were ground in 1 \times cell lysis buffer at a ratio of 0.1 g tissue per 0.1 mL. The supernatant of tumor tissue-lysis buffer was collected after centrifugation at 13 800g for 10 min. The whole-cell lysate and whole-tumor lysate supernatants were prepared and quantified with a BCA protein kit (Thermo). After preparations of protein samples, 10–40 μ g of protein of each sample was loaded on 10% polyacrylamide SDS-PAGE gels and transferred to PVDF membranes (Millipore). β -Actin was used as an internal reference. The protein bands were visualized using an enhanced chemiluminescence western blot detection system (GE AI600) and quantified with the Image Quant TL software.

2.12 Statistical analysis

All experiments were performed at least three times and data expressed as means \pm standard deviation (SD). Statistical significance was determined using one-way analysis of variance (ANOVA) and Tukey's test: * $p < 0.05$ was considered statistically significant, ** $p < 0.01$ was considered highly significant, *** $p < 0.001$ was considered extremely significant.

3. Results and discussion

3.1 Preparation and characterization of PLG-g-mPEG/CA4

Firstly, PLG-g-mPEG/CA4 was synthesized through the Yamaguchi reaction as shown in Fig. 1A. The chemical structure of PLG-g-mPEG/CA4 was confirmed by ¹H NMR (Fig. 1B). The appearance of characteristic peaks at δ 6.58 (k + l + m), 6.44 (j) and 6.27 (h + i) ppm were attributed to the presence of CA4 moieties, which indicated that PLG-g-mPEG/CA4 was synthesized successfully. M_n and M_w/M_n of PLG-g-mPEG/CA4 were 8.1×10^4 g mol⁻¹ and 1.71, respectively, ascertained by gel permeation chromatography. PLG-g-mPEG/CA4 and free CA4 contents were measured using HPLC with a UV-Vis detector. Drug loading content (DLC%) was 25.6 wt% and free CA4 was 0.01 wt%. PLG-g-mPEG/CA4 formed nanoparticles by self-assembly in aqueous solution. The diameter of the CA4-NPs was 91.1 ± 0.9 nm determined by DLS (Fig. 1C). The quantity of CA4 released in pH 7.4, pH 6.8 or pH 5.0 PBS buffer was quantified by HPLC using a UV-Vis detector, as shown in Fig. 1D. CA4 release from CA4-NPs was $64.9 \pm 3.0\%$ at 72 h in pH 7.4 PBS buffer, greater than in pH 6.8 PBS buffer ($34.3 \pm 2.7\%$) and in pH 5.0 PBS buffer ($8.5 \pm 1.9\%$). The slow CA4 release at lower pH might be attributed to the significantly increased protonation degree of the carboxyl residues in mPEG-g-PLG polymer, resulting in a more compact CA4-NPs core.

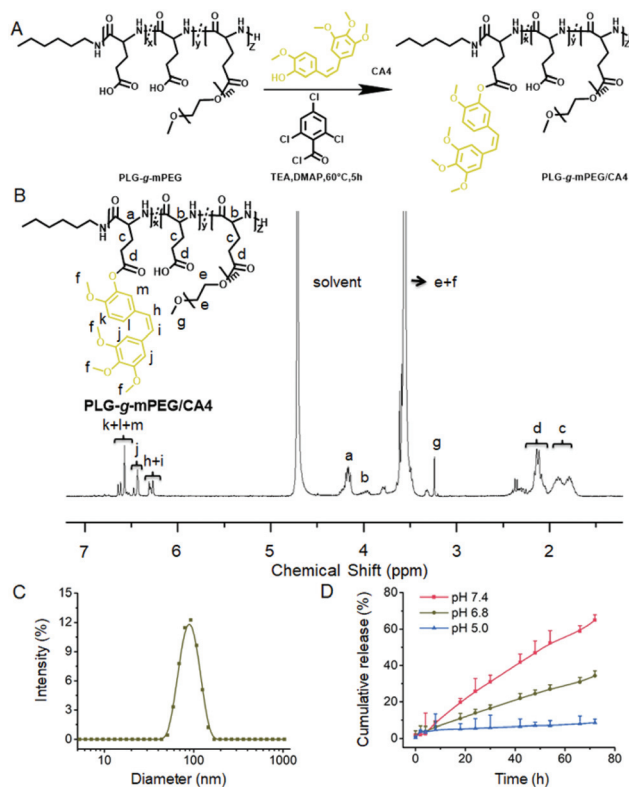


Fig. 1 (A) Synthesis of PLG-g-mPEG/CA4. (B) ¹H NMR spectrum of PLG-g-mPEG/CA4 in D₂O. (C) Diameter of CA4-NPs determined by DLS. (D) Release of CA4 from CA4-NPs in PBS buffer at different pH values ($n = 3$).

3.2 CA4-NPs induce CXCR4 overexpression in tumor tissues

Then, the CXCR4 expression induced by CA4-NPs treatment was investigated in the orthotopic 4T1 mammary carcinoma mouse model. CA4-NPs treatment increased the expression of CXCR4 remarkably in tumor tissues as analyzed by immunofluorescence staining assay. A significant increase in CXCR4 expression was observed in the CA4-NPs group compared with the PBS group. At 24 h or 48 h post-injection, the fluorescence intensity of CXCR4 in the CA4-NPs (60) group was higher than that in the CA4-NPs (30) group, and the fluorescence intensity of CXCR4 in the CA4-NPs (30) group was higher than that in the PBS group. These results showed that the CXCR4 expression in tumor tissues was dependent on CA4-NPs doses. The fluorescence intensities of CXCR4 in CA4-NPs (30) and CA4-NPs (60) groups at 48 h were higher than those at 24 h, indicating that the CXCR4 expression in tumor tissues was time-dependent (Fig. 2A and B). The relative protein expression of CXCR4 in the CA4-NPs (30) group was 1.5-fold ($p < 0.05$) of that in the PBS group and the expression of CXCR4 in the CA4-NPs (60) group was 2.8-fold ($p < 0.01$) of that in the PBS group after 48 h post treatment analyzed by western blotting (Fig. 3). All these results gave the evidence that the expression of CXCR4 was increased in tumor tissues after CA4-NPs treatment.

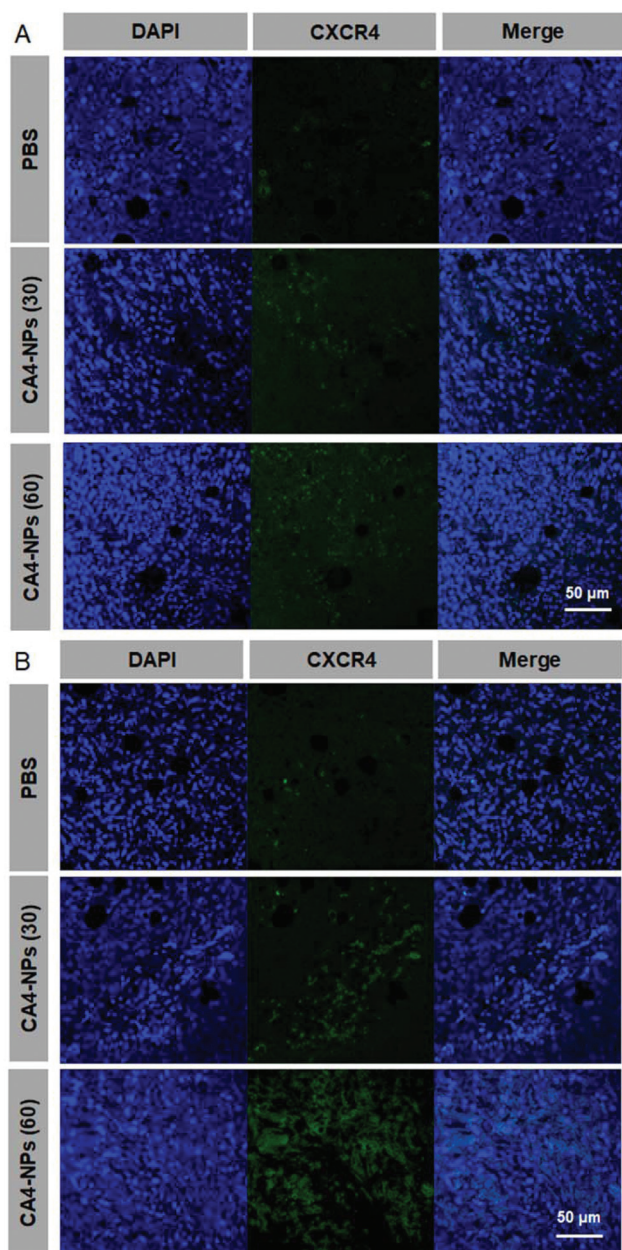


Fig. 2 Immunofluorescence staining for CXCR4 of tumor tissues. (A) The tumor tissues ($\sim 150 \text{ mm}^3$) were analyzed after 24 h post treatment. (B) The tumor tissues ($\sim 150 \text{ mm}^3$) were analyzed after 48 h post treatment. CA4-NPs (30) represented that the dose of CA4-NPs was 30 mg kg^{-1} on CA4 basis, and CA4-NPs (60) represented that the dose of CA4-NPs was 60 mg kg^{-1} on the CA4 basis. Scale bar represents $50 \mu\text{m}$.

3.3 Hypoxia induced by CA4-NPs

Next, we analyzed the factors in inducing the CXCR4 overexpression in tumor tissues after CA4-NPs treatment. Considering that CA4-NPs treatment could induce a severe hypoxic microenvironment in solid tumors²⁰ and the expression of CXCR4 in tumor tissues could be regulated by hypoxia,^{30,31} the overexpression of CXCR4 in tumor tissues might be regulated by hypoxia induced by CA4-NPs treatment.

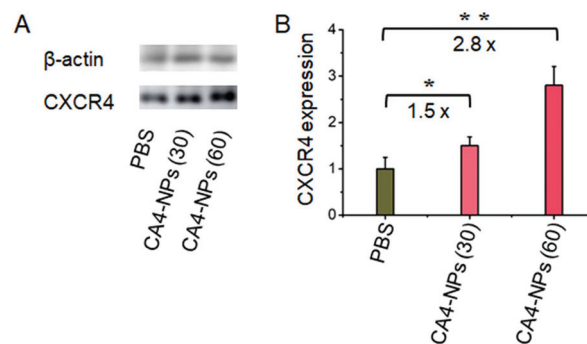


Fig. 3 (A) The expression of CXCR4 in tumor tissues was measured by western blotting. (B) The quantification analysis of the expression of CXCR4 in tumor tissues measured by western blotting ($n = 3$). The tumor tissues ($\sim 150 \text{ mm}^3$) were analyzed 48 h post treatment. CA4-NPs (30) represented that the dose of CA4-NPs was 30 mg kg^{-1} on the CA4 basis, and CA4-NPs (60) represented that the dose of CA4-NPs was 60 mg kg^{-1} on the CA4 basis. In (B), the CXCR4 level in the tumor tissues of the PBS group represents the reference value. Data represent means \pm SD, statistical analysis by one-way analysis of variance (ANOVA) and Tukey's test: * $p < 0.05$; ** $p < 0.01$; and *** $p < 0.001$.

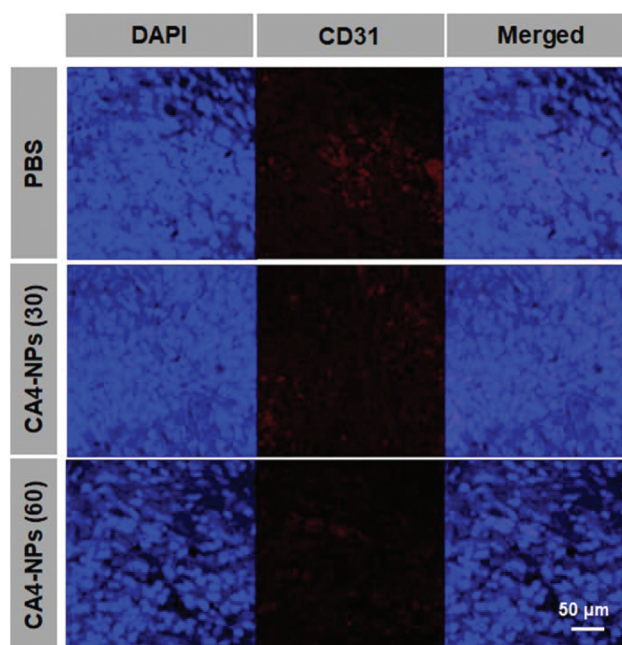


Fig. 4 Immunofluorescence staining for CD31 of tumor tissues 48 h post treatment. CA4-NPs (30) represented that the dose of CA4-NPs was 30 mg kg^{-1} on the CA4 basis, and CA4-NPs (60) represented that the dose of CA4-NPs was 60 mg kg^{-1} on the CA4 basis. Scale bar represents $50 \mu\text{m}$.

So, we first investigated the vascular state after 48 h post-injection of CA4-NPs. The immunofluorescence staining of CD31 indicated that the vascular density in the CA4-NPs (60) group was lower than that in the CA4-NPs (30) group, and the vascular density in the CA4-NPs (30) group was lower than that in the PBS group (Fig. 4). These results showed that CA4-NPs performed strong dose-dependent vascular disruption in tumor

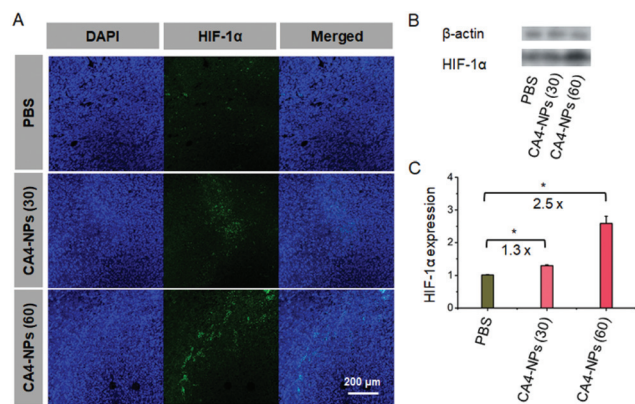


Fig. 5 (A) Immunofluorescence staining for HIF-1 α of tumor tissues 48 h post treatment. (B) The relative expression of HIF-1 α in tumor tissues measured by western blotting. (C) The quantification analysis of the expression of HIF-1 α in tumor tissues measured by western blotting ($n = 3$). CA4-NPs (30) represented that the dose of CA4-NPs was 30 mg kg⁻¹ on the CA4 basis, and CA4-NPs (60) represented that the dose of CA4-NPs was 60 mg kg⁻¹ on the CA4 basis. Scale bar represents 200 μ m. Data represent means \pm SD, statistical analysis by one-way analysis of variance (ANOVA) and Tukey's test: * $p < 0.05$; ** $p < 0.01$; and *** $p < 0.001$.

tissues. Then, we compared the level of HIF-1 α in 4T1 tumor tissues under different treatments. CA4-NPs treatment increased the expression of HIF-1 α in tumor tissues significantly (Fig. 5A). The level of HIF-1 α in the CA4-NPs (30) group was 1.3-fold ($p < 0.05$) of that in the PBS group, and the level of HIF-1 α in the CA4-NPs (60) group was 2.5-fold ($p < 0.05$) of that in the PBS group after 48 h intravenous injection (Fig. 5B and C) as analyzed by western blotting.

These results revealed that CA4-NPs treatment could block the vessel, induce severe hypoxic conditions and high expression of HIF-1 α in tumor tissues.

3.4 Hypoxia induces HIF-1 α increase in 4T1 cells

To ascertain the influence of hypoxic conditions on the expression of HIF-1 α in 4T1 cells, we further compared the expression of HIF-1 α in 4T1 tumor cells cultured under normoxic (20% oxygen) or simulate hypoxic (1% oxygen) conditions. After culturing at different oxygen conditions for 48 h, the relative protein expression of HIF-1 α in the hypoxic (1% oxygen) group was 1.8-fold ($p < 0.01$) of that in the normoxic (20% oxygen) group (Fig. 6A and B) measured by western blot analysis. The relative HIF-1 α mRNA expression in the hypoxic group was 3.4-fold ($p < 0.001$) of that in the normoxic (20% oxygen) group (Fig. 6C). The results indicated that hypoxic conditions could induce the expression of HIF-1 α increase in 4T1 cells.

3.5 Hypoxia induces CXCR4 overexpression in 4T1 cells

To further verify that whether the hypoxic condition could induce the expression of CXCR4 increase in 4T1 tumor cells. The 4T1 cells were cultured under normoxic (20% oxygen) and simulated hypoxic (1% oxygen) conditions for 48 h. The rela-

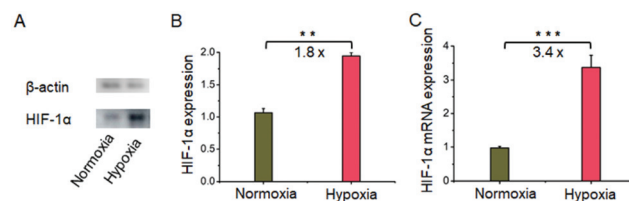


Fig. 6 (A) The relative expression of HIF-1 α in 4T1 cells measured by western blotting. (B) The quantification analysis of the expression of HIF-1 α in 4T1 cells measured by western blotting ($n = 3$). (C) The relative expression of HIF-1 α mRNA in 4T1 cells measured by RT-PCR. The 4T1 cells were analyzed after culturing under normoxic (20% oxygen) and simulated hypoxic (1% oxygen) conditions for 48 h. Data represent means \pm SD, statistical analysis by one-way analysis of variance (ANOVA) and Tukey's test: * $p < 0.05$; ** $p < 0.01$; and *** $p < 0.001$.

tive protein expression of CXCR4 in the hypoxic group was 1.6-fold ($p < 0.05$) of that in the normoxic (20% oxygen) group (Fig. 7A and B) measured by western blot analysis. The relative CXCR4 mRNA expression in the hypoxic group was 3.5-fold ($p < 0.001$) of that in the normoxic (20% oxygen) group (Fig. 7C). The relative expression of CXCR4 in 4T1 cells was also analyzed by immunofluorescence staining (Fig. 8). The fluorescence intensity of CXCR4 in the hypoxic group was higher than that in the normoxic group. All these results indicated that the hypoxic condition could increase the expression of CXCR4.

3.6 Combining PLF with CA4-NPs for tumor growth inhibition

Because of the overexpression of CXCR4 in tumor tissues induced by hypoxic microenvironment after CA4-NPs treatment, the metastasis of tumor cells would occur. To address this serious problem, we combined CXCR4 antagonist, plerixafor, with CA4-NPs for tumor growth and metastasis inhibition simultaneously. An orthotopic 4T1 mammary adenocarcinoma mouse model was established on female BALB/c mice as described above.

When the tumor volume reached about 150 mm³, the mice were randomly divided into 6 groups: PBS; PLF (2.5 mg kg⁻¹ on PLF basis), termed PLF; CA4-NPs (30 mg kg⁻¹ on CA4

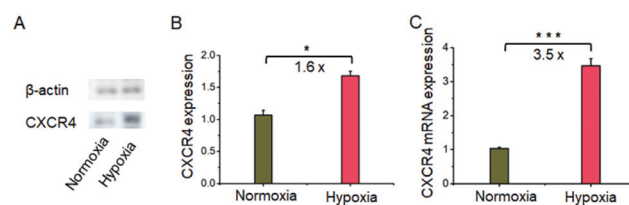


Fig. 7 (A) The relative expression of CXCR4 in 4T1 cells measured by western blotting. (B) The quantification analysis of the expression of CXCR4 in tumor cells measured by western blotting ($n = 3$). (C) The expression of CXCR4 mRNA in 4T1 cells measured by RT-PCR ($n = 3$). The 4T1 cells were analyzed after culturing under normoxic (20% oxygen) and simulated hypoxic (1% oxygen) conditions for 48 h. Data represent means \pm SD, statistical analysis by one-way analysis of variance (ANOVA) and Tukey's test: * $p < 0.05$; ** $p < 0.01$; and *** $p < 0.001$.

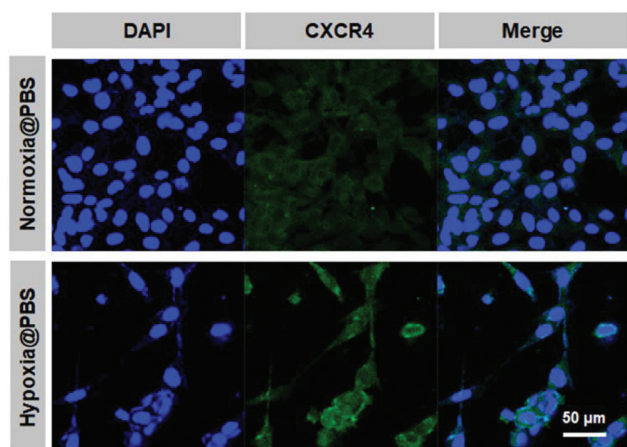


Fig. 8 Immunofluorescence staining for CXCR4 of 4T1 cells. The 4T1 cells were analyzed after culturing under normoxic (20% oxygen) and simulated hypoxic (1% oxygen) conditions for 48 h. Scale bar represents 50 μm.

basis), termed CA4-NPs (30); CA4-NPs (30 mg kg⁻¹ on CA4 basis) + PLF (2.5 mg kg⁻¹ on PLF basis), termed CA4-NPs (30) + PLF; CA4-NPs (60 mg kg⁻¹ on CA4 basis), termed CA4-NPs (60); CA4-NPs (60 mg kg⁻¹ on CA4 basis) + PLF (2.5 mg kg⁻¹ on PLF basis), termed CA4-NPs (60) + PLF. The treatment regimen showed that CA4-NPs (30) were injected at day 1 and day 7 *via* intravenous injection (i.v.), CA4-NPs (60) were injected at day 1 *via* intravenous injection (i.v.) and PLF was injected everyday *via* intraperitoneal injection (i.p.) (Fig. 9A). Tumor volume change and body weight variation of the mice were observed for 13 days. Monotherapies with either PLF or CA4-NPs (30)

demonstrated a mild effect of tumor growth inhibition. The mean tumor volumes were 716 ± 244 mm³ and 1025 ± 437 mm³, while tumor inhibition rates were 38.4% and 11.8% for the PLF and CA4-NPs (30) monotherapy groups, respectively. The mean tumor volume was 570 ± 130 mm³, and the tumor inhibition rate was 51.0% for the CA4-NPs (30) + PLF group. The CA4-NPs (30) + PLF group demonstrated a higher tumor growth inhibition effect compared to the monotherapy CA4-NPs (30) group and PLF group. The CA4-NPs (60) group showed a mean tumor volume of 377 ± 153 mm³ and a tumor inhibition rate of 67.6%, respectively. This revealed that increasing the dose of CA4-NPs would inhibit tumor growth effectively. The combination therapy with CA4-NPs (60) and PLF inhibited tumor growth more significantly compared to that with the CA4-NPs (60) monotherapy group. The mean tumor size of the CA4-NPs (60) + PLF group was 101 ± 49 mm³ at the end point and the tumor inhibition rate was 91.3%, a 1.4-fold compared to that of the CA4-NPs (60) group (Fig. 9B and C). The *Q* value was 2.00, which was higher than 1.15, indicating a synergistic effect of the combination CA4-NPs (60) with PLF for antitumor efficacy. The body weight was monitored for the assessment of systemic toxicity in the treated mice (Fig. 9D). There was no body weight loss significantly in the PLF group compared with the PBS group. Body weight decreased in the CA4-NPs (60) group during the early time points (~11%) and recovered after 7 days gradually. In the CA4-NPs (60) + PLF group, body weight decreased (~11%) and gradually recovered after 13 days. These results revealed that the combination treatment with CA4-NPs (60) + PLF exhibited significantly enhanced antitumor efficacy and minimal systemic toxicity when compared with monotherapy controls.

3.7 Combining PLF with CA4-NPs for tumor metastasis inhibition

To investigate the tumor metastasis inhibition of the cooperative strategy, pulmonary metastatic nodules were observed. Lungs were injected tracheally with India ink and destained in Fekete's solution at the end point of the treatment. The white pulmonary metastasis foci were photographed (Fig. 10A) and counted (Fig. 10B). The pulmonary metastatic nodules in the CA4-NPs (60) + PLF group were barely observable and the lung size was normal. The pulmonary metastasis foci in the CA4-NPs (30) group were 3.8-fold (*p* < 0.001) of that in the CA4-NPs (60) + PLF group. The pulmonary metastasis foci in the PBS group were 22.4-fold (*p* < 0.001) of that in the CA4-NPs (60) + PLF group. The pulmonary metastasis foci in the PLF group were 6.43-fold (*p* < 0.001) of that in the CA4-NPs (60) + PLF group. The pulmonary metastasis foci in the CA4-NPs (30) + PLF group were 3.71-fold (*p* < 0.01) of that in the CA4-NPs (60) + PLF group and the pulmonary metastasis foci in the CA4-NPs (60) group were 2.29-fold (*p* < 0.05) of that in the CA4-NPs (60) + PLF group. The H&E staining micrographs showed a similar metastasis inhibition effect of the combination group (Fig. 10C). All these results revealed that combining PLF with CA4-NPs treatment could inhibit metastasis significantly.

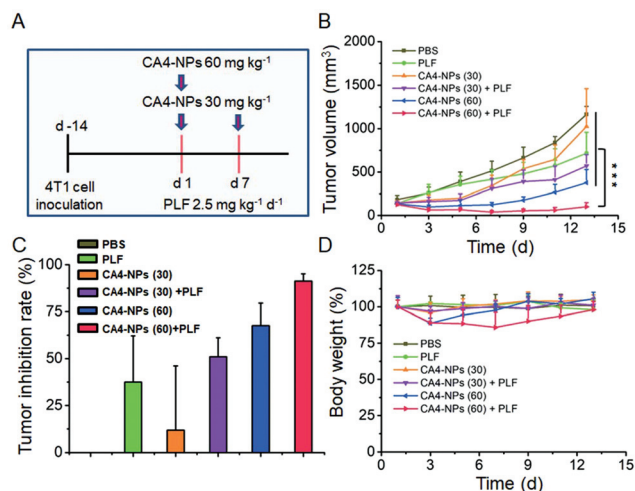


Fig. 9 (A) Treatment scheme of orthotopic 4T1 tumors with CA4-NPs and PLF (*n* = 6 mice per group). (B) Change in tumor volume during treatment. Dose of PLF was 2.5 mg kg⁻¹, dose of CA4 was 30 mg kg⁻¹ or 60 mg kg⁻¹. Data represent means ± SD, statistical analysis by one-way analysis of variance (ANOVA) and Tukey's test: **p* < 0.05; ***p* < 0.01; and ****p* < 0.001. (C) Tumor inhibition rate in the orthotopic 4T1 tumor model. (D) Change in body weight in the 4T1 tumor model.

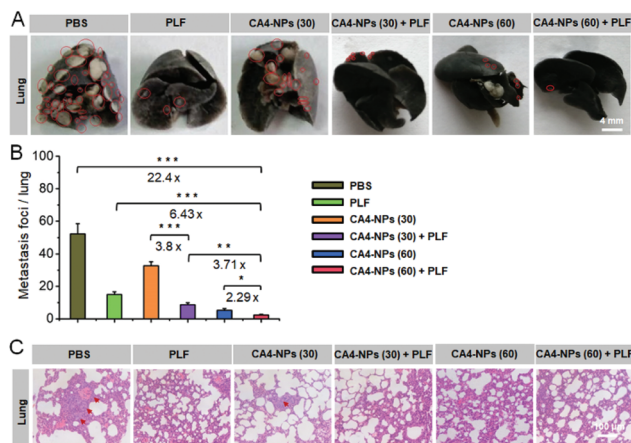


Fig. 10 (A) The lungs of different groups were injected with India ink at the end point of the treatment. Scale bar represents 4 mm. (B) Number of lung metastasis foci from different treatment groups ($n = 3$). Data represent means \pm SD, statistical analysis by one-way analysis of variance (ANOVA) and Tukey's test: * $p < 0.05$; ** $p < 0.01$; and *** $p < 0.001$. (C) H&E staining of lung sections from different treatment groups. Red arrow represents micrometastasis. The scale bar represents 100 μm .

3.8 Histological analysis

To evaluate the anti-tumor effects and cytotoxicity on normal organs of the treatment, tumors and normal organs were excised and stained with hematoxylin and eosin (H&E). As shown in Fig. 11, a larger proportion of dead cells in tumors in the CA4-NPs (60) + PLF group was observed compared with other groups, and the cells were characterized with small, fragmented nuclei and hyper-eosinophilic cytoplasm. CA4-NPs (60) and CA4-NPs (30) + PLF groups showed a similar therapy effect, but weaker than that of the CA4-NPs (60) + PLF group. PLF and CA4-NPs (30) groups displayed a similar antitumor effect, which was weaker than that of the CA4-NPs (30) + PLF group. These tumor histology results were consistent with that of the tumor volume change. Furthermore, there were no unusual pathological abnormalities in normal organs in any

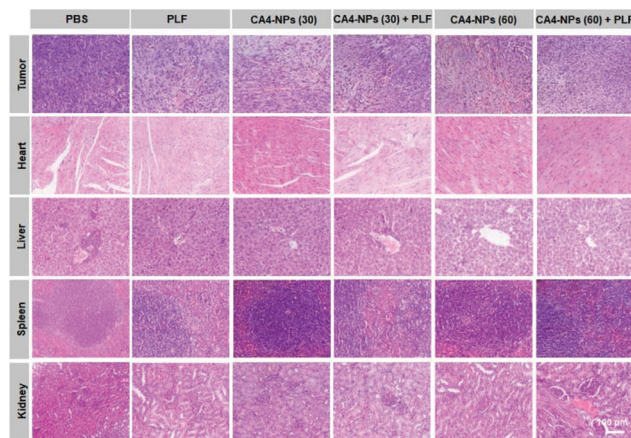


Fig. 11 H&E staining of different tissues after the treatment of 4T1-bearing mice with different treatments. Scale bar represents 100 μm .

group stained with H&E, such as the heart, kidney, *etc.* All the results revealed that CA4-NPs + PLF combination treatment could strongly increase the antitumor effect without significant systematic cytotoxicity on normal organs.

4. Conclusions

In summary, we developed a cooperative strategy through combining CA4-NPs with PLF to improve the tumor growth and metastasis inhibition effect simultaneously. The use of CA4-NPs was aimed to selectively disrupt new blood vessels in tumor tissues for targeting tumor therapy. However, the level of CXCR4 in tumor tissues was increased after CA4-NPs treatment, which was confirmed by immunofluorescence staining and western blot analysis. Then, we verified that CA4-NPs-induced CXCR4-signal-overexpression resulted in a severe hypoxic tumoral microenvironment induced by CA4-NPs treatment. The combination of CA4-NPs + PLF exhibited a significantly improved tumor inhibition rate and decreased tumor cell metastasis compared with monotherapies. Herein, PLF, as a CXCR4 antagonist, could disrupt the CXCR4/CXCL12 axis and inhibit tumor cell metastasis. This work gave evidence for the concept that the blocking of the CXCR4/CXCL12 axis with plerixafor during CA4-NPs treatment would serve as a promising strategy for improving tumor therapy and inhibiting metastasis simultaneously. Considering that all VDA treatment would cause a severe hypoxic tumoral microenvironment and then CXCR4 expression increase, the combination therapy strategy of VDAs + CXCR4 antagonists should have great potential in inhibiting tumor growth and metastasis simultaneously in cancer treatment.

Conflicts of interest

There are no conflicts to declare.

Acknowledgements

This work was financially supported by the National Natural Science Foundation of China (Projects 51503202, 51673189, and 51873206), the Ministry of Science and Technology of China (Projects 2018ZX09711003-012) and the Jilin Province (20190103033JH).

Notes and references

- 1 C. L. Chaffer and R. A. Weinberg, *Science*, 2011, **331**, 1559–1564.
- 2 L. A. Torre, R. L. Siegel, E. M. Ward and A. Jemal, *Cancer Epidemiol., Biomarkers Prev.*, 2016, **25**, 16–27.
- 3 D. Zhang, B. Li, J. Shi, L. Zhao, X. Zhang, C. Wang, S. Hou, W. Qian, G. Kou, H. Wang and Y. Guo, *Cancer Res.*, 2010, **70**, 2495–2503.

- 4 J. Su, H. Sun, Q. Meng, Q. Yin, S. Tang, P. Zhang, Y. Chen, Z. Zhang, H. Yu and Y. Li, *Adv. Funct. Mater.*, 2016, **26**, 1243–1252.
- 5 M. Shen, Y.-Z. Jiang, Y. Wei, B. Ell, X. Sheng, M. Esposito, J. Kang, X. Hang, H. Zheng, M. Rowicki, L. Zhang, W. J. Shih, T. Celia-Terrassa, Y. Liu, I. Cristea, Z.-M. Shao and Y. Kang, *Cancer Cell*, 2019, **35**, 64–80.e7.
- 6 S. Habringer, C. Lapa, P. Herhaus, M. Schottelius, R. Istvanffy, K. Steiger, J. Slotta-Huspenina, A. Schirbel, H. Haenscheid, S. Kircher, A. K. Buck, K. Goetze, B. Vick, I. Jeremias, M. Schwaiger, C. Peschel, R. Oostendorp, H.-J. Wester, G.-U. Grigoleit and U. Keller, *Theranostics*, 2018, **8**, 369–383.
- 7 Z. Wang, Y. Ma, X. Yu, Q. Niu, Z. Han, H. Wang, T. Li, D. Fu, S. Achilefu, Z. Qian and Y. Gu, *Adv. Funct. Mater.*, 2018, **28**, 1800732.
- 8 C. T. Veldkamp, J. J. Ziarek, F. C. Peterson, Y. Chen and B. F. Volkman, *J. Am. Chem. Soc.*, 2010, **132**, 7242–7243.
- 9 R. Diaz, L. Sanchez-Garcia, N. Serna, A. Sanchez-Chardi, O. Cano-Garrido, J. M. Sanchez, U. Unzueta, E. Vazquez and A. Villaverde, *Sci. China Mater.*, 2019, **62**, 892–898.
- 10 C. H. Wu, J. S. Song, H. H. Kuan, S. H. Wu, M. C. Chou, J. J. Jan, L. K. Tsou, Y. Y. Ke, C. T. Chen, K. C. Yeh, S. Y. Wang, T. K. Yeh, C. T. Tseng, C. L. Huang, M. H. Wu, P. C. Kuo, C. J. Lee and K. S. Shia, *J. Med. Chem.*, 2018, **61**, 818–833.
- 11 D. Dutta, K. Hickey, M. Salifu, C. Fauer, C. Willingham and S. E. Stabenfeldt, *Biomater. Sci.*, 2017, **5**, 1640–1651.
- 12 P. Staller, J. Sulitkova, J. Liszlwan, H. Moch, E. J. Oakeley and W. Krek, *Nature*, 2003, **425**, 307–311.
- 13 M. Gil, M. Seshadri, M. P. Komorowski, S. I. Abrams and D. Kozbor, *Proc. Natl. Acad. Sci. U. S. A.*, 2013, **110**, E1291–E1300.
- 14 G. M. Tozer, C. Kanthou and B. C. Baguley, *Nat. Rev. Cancer*, 2005, **5**, 423–435.
- 15 M. M. Cooney, W. van Heeckeren, S. Bhakta, J. Ortiz and S. C. Remick, *Nat. Clin. Pract. Oncol.*, 2006, **3**, 682–692.
- 16 Z. Liu, N. Shen, Z. Tang, D. Zhang, L. Ma, C. Yang and X. Chen, *Biomater. Sci.*, 2019, **7**, 2803–2811.
- 17 S. J. Lunt, S. Akerman, S. A. Hill, M. Fisher, V. J. Wright, C. C. Reyes-Aldasoro, G. M. Tozer and C. Kanthou, *Int. J. Cancer*, 2011, **129**, 1979–1989.
- 18 Q. Chen, G. Liu, S. Liu, H. Su, Y. Wang, J. Li and C. Luo, *Trends Pharmacol. Sci.*, 2018, **39**, 59–74.
- 19 W. Song, Z. Tang, D. Zhang, H. Yu and X. Chen, *Small*, 2015, **11**, 3755–3761.
- 20 S. Yang, Z. Tang, C. Hu, D. Zhang, N. Shen, H. Yu and X. Chen, *Adv. Mater.*, 2019, **31**, 1805955.
- 21 T. Liu, D. Zhang, W. Song, Z. Tang, J. Zhu, Z. Ma, X. Wang, X. Chen and T. Tong, *Acta Biomater.*, 2017, **53**, 179–189.
- 22 J. Jiang, N. Shen, T. Ci, Z. Tang, Z. Gu, G. Li and X. Chen, *Adv. Mater.*, 2019, DOI: 10.1002/adma.201904278.
- 23 Z. Tang and X. Chen, *Acta Polym. Sin.*, 2019, 543–552.
- 24 S. M. Devine, N. Flomenberg, D. H. Vesole, J. Liesveld, D. Weisdorf, K. Badel, G. Calandra and J. F. DiPersio, *J. Clin. Oncol.*, 2004, **22**, 1095–1102.
- 25 J. F. DiPersio, I. N. Micallef, P. J. Stiff, B. J. Bolwell, R. T. Maziarz, E. Jacobsen, A. Nademanee, J. McCarty, G. Bridger, G. Calandra and Investigators, *J. Clin. Oncol.*, 2009, **27**, 4767–4773.
- 26 H. Yu, Z. Tang, D. Zhang, W. Song, Y. Zhang, Y. Yang, Z. Ahmad and X. Chen, *J. Controlled Release*, 2015, **205**, 89–97.
- 27 P. Hang, Z. W. Liu, G. G. Zhang, Y. S. Xiao, H. Xu and J. L. Wang, *J. Pract. Med.*, 2014, **5**, 738–741.
- 28 W. Qi, B. A. Davidson, M. Nguyen, T. Lindstrom, R. J. Grey, R. Burnett, E. Aflaki, E. Sidransky and W. Westbroek, *Biochem. J.*, 2019, **476**, 261–274.
- 29 Z. Q. Liu, T. Mahmood and P. C. Yang, *N. Am. J. Med. Sci.*, 2014, **6**, 160–160.
- 30 L. Dong, S. You, Q. Zhang, S. Osuka, N. S. Devi, S. Kaluz, J. H. Ferguson, H. Yang, G. Chen, B. Wang, H. E. Grossniklaus and E. G. Van Meir, *Clin. Cancer Res.*, 2019, **25**, 2206–2218.
- 31 G. Guan, Y. Zhang, Y. Lu, L. Liu, D. Shi, Y. Wen, L. Yang, Q. Ma, T. Liu, X. Zhu, X. Qiu and Y. Zhou, *Cancer Lett.*, 2015, **357**, 254–264.